Methods to investigate the RPV exterior two-phase flow behavior in the event of a core melt

H. Schmidt[1], W. Brettschuh[1], J. Meseth[1], E. Friesen[1], O. Herbst[1], W. Kastner[1], W. Köhler[1] and J.Miettinen[2]

[1]Siemens Nuclear Power GmbH,
P.O. Box 3220, 91050 Erlangen, Germany
Tel.: +49 9131 18 3718
Fax: +49 9131 18 2851
E-mail: Holger.Schmidt@erl11.siemens.de

[2]Technical Research Centre of Finland

1 Introduction

Siemens Nuclear Power (SNP) develops a new boiling water reactor called SWR 1000. It's safety concept will consist of passive safety equipment combined with active systems, and through this diversity, meets the goal of reducing the probability of core damage compared to existing plants. Furthermore, the design is aimed at being able to control a postulated core melt accident to such an extent that the consequences of an accident remain restricted to the plant. The core melt is retained in the Reactor Pressure Vessel (RPV) at low pressure owing to cooling of the RPV exterior. For this purpose a passive flooding system is installed which feeds into the lower area of the drywell from the core flooding pool by gravity. The water will penetrate through apertures in the RPV-insulation in the gap between the insulation and the RPV- wall as it is schematically shown in Fig. 1.

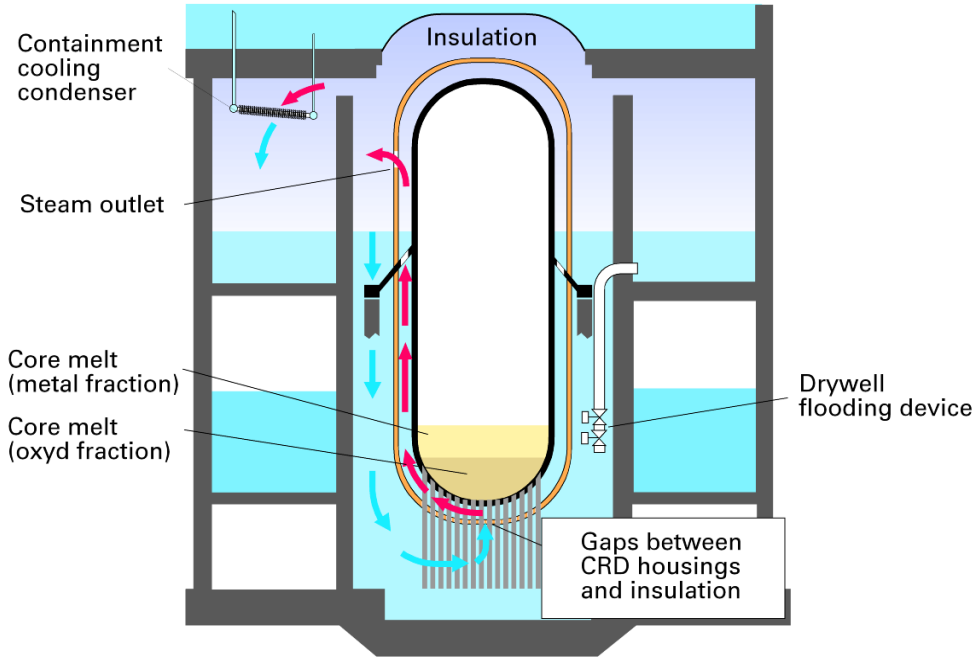

Fig. 1: Scheme of the exterior vessel cooling concept

SNP performs – in co-operation with the Technical Research Centre of Finland (VTT) - tests to quantify the safety margins of the exterior cooling concept of the SWR 1000. A Siemens internal investigation proves that the heat fluxes through the wall will be distributed in such a way that the minimal heat flux will be at the bottom of the RPV. The maximum will be in the spherical part of the RPV with an inclination of almost 50°. The in the literature /1/ to /13/ mentioned critical heat fluxes for comparable configurations are in the range of 300 to 500 kW/m² at the bottom and 1000 to 1500 kW/m² at the side and are almost five times higher than the calculated heat fluxes through the RPV wall. The comparison of literature values and heat fluxes through the RPV indicates high safety margins. Anyhow, the influence of the control rod drive (CRD) housing is unknown. It is the aim of the investigation to demonstrate the functioning of the exterior cooling concept and to quantify the safety margins.

The heat transfer conditions will be very complex. The local heat transfer as well as the global flow behavior may influence the critical heat fluxes (CHF). For that reason it is planned to measure critical heat fluxes in a section model with a 1:1 scaling. The flow and heat transfer conditions will be decoupled in order to prove that the section is representative. The procedure contains three different kinds of tests which are mentioned in Fig. 2 and which are described in the following:

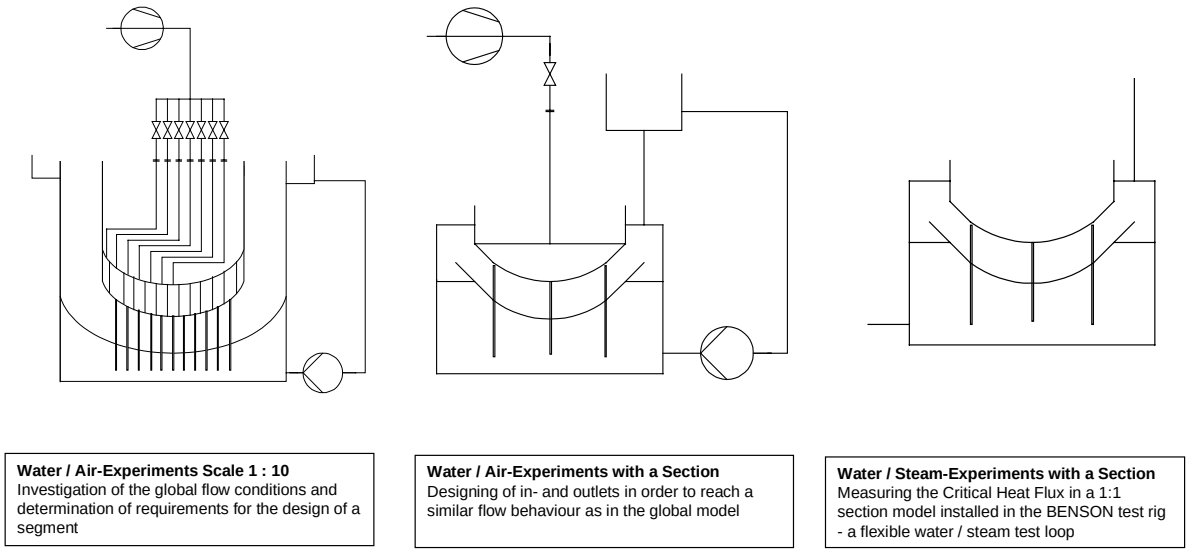

Fig. 2: Decoupling of flow conditions and heat transfer

- Investigation on the flow conditions in a global model
  The aim of the tests with a water/air operated global model is to describe the flow behavior in the gap between the insulation and the RPV and to have a data base to validate or to adapt programs.
- Investigation on the flow conditions in a segment model
  The aim of the tests is to prove that the flow in segment is similar to flow in the global model.
- Measurement of Safety Margins
  The aim of the tests is to measure the CHF up to three times of the heat fluxes which would occur in the event of a hypothetical core melt accident. A segment model will be installed in the BENSON test rig in order to supply it with water of pressure

between 4 and 1,3 bar and a subcooling of 0 to 10 K. The segment model will be heated and the CHF will be identified based on temperature measurements of the wall.

The tests to investigate the flow conditions in the global model are finished. A Laser-Doppler-Anemometer has been used to measure the liquid velocities. The void fraction was determined using a fiber optical needle probe and impedance probes. Mass balances performed based on the measurements prove the plausibility of the applied methods.

2 Setup of the global model

It is the aim of the tests with the global flow model to investigate the flow behavior in the case of the exterior cooling by performing water/air experiments. Fig. 3 shows the model which size is 1:10. The main components are the simulated RPV and the insulation, which is made of a transparent material. The internal pumps and control rod drive housings are simulated by transparent bars. The bottom of the simulated RPV is made of a porous structure. In order to simulate boiling on the outer surface of the RPV air was pressed through this material. The setup of the RPV consists eight rotational symmetric chambers in order to simulate the in chapter 1 mentioned heat flux distribution. Each of the chambers has an own air supply and the air mass flow can be adjusted individually.

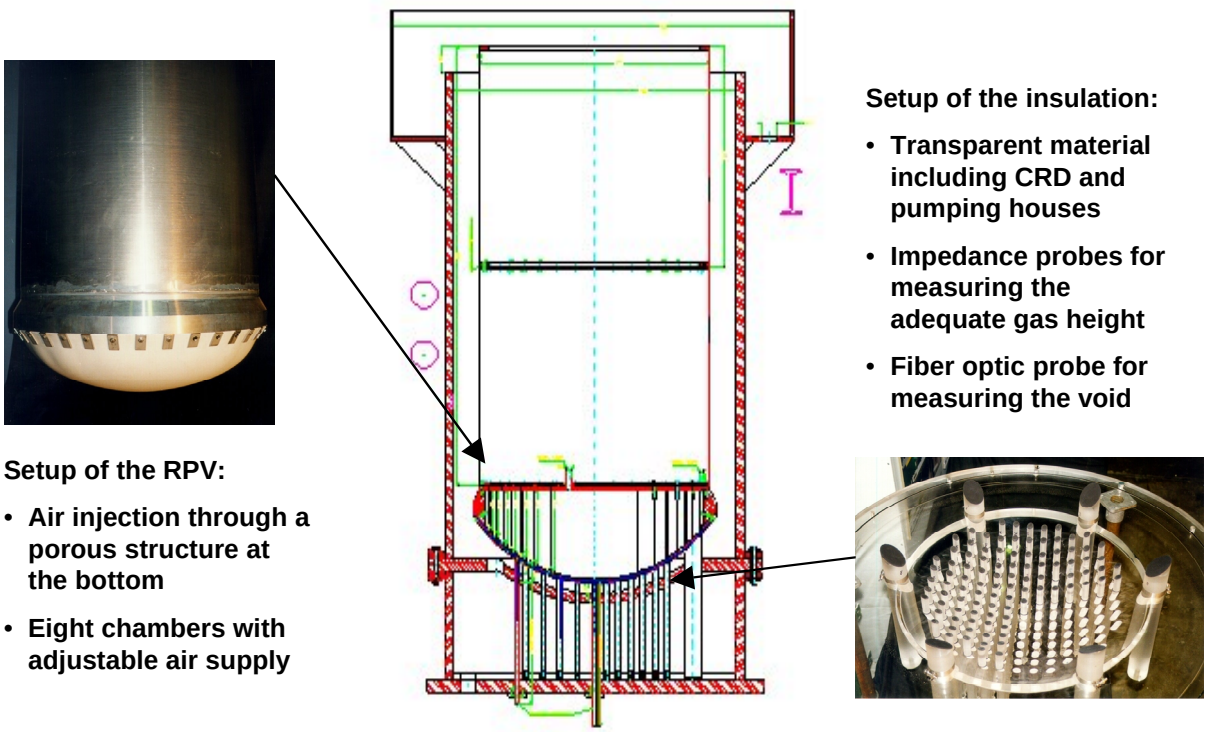

Fig. 3: Global model

3 Phenomenology

Based on visual observation the following impression of the flow behavior was received: The main characteristica are the circulation and the counter-current flow at the bottom of the RPV as it is schematically shown in Fig. 4. One can see that the water/air mixture flows around the calotte of the RPV. Opposite to the direction of the mixture flow one can see a single-phase water flow along the insulation. This proves that water will flow in the direction of the source (heat or in the case of the tests injection). By observing small sized bubbles one has the impression as if water penetrates during the counter-current flow into the water/air mixture. A view from a position below the model in the direction of the RPV gave the impression as if the flow is rotational symmetric and as if there are no preference directions of the water/air flow. The performed measurements underline the visual observation based description of the global flow behavior.

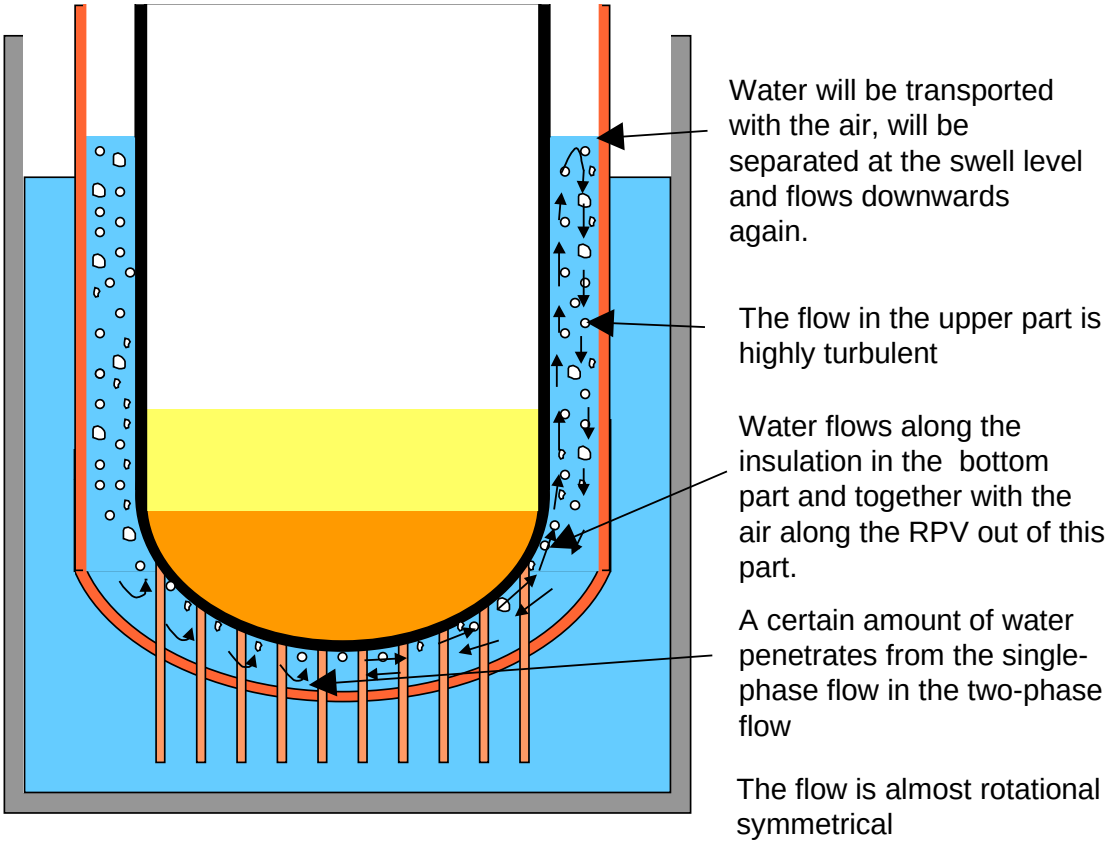

Fig. 4: Phenomenology

4 Measurement techniques

The following three different measurement techniques have been used to investigate the flow around the RPV:

- Fiber optical needle probe – to measure the local void fraction at some positions
- Impedance probes – to measure an averaged void fraction

- Laser-Doppler-Anemometer – to measure local velocities.

4.1 Fiber optical needle probe measurements

Fig. 5 shows the fiber optical needle probe which has been delivered by the Technical University of Darmstadt /14/. It is designed in such a way that the probe can be moved in the direction of the axis of the surrounding tube, that has an outer diameter of the simulated CRD-housings. It has been installed instead of one of the transparent bares as they are shown in Fig. 3. The needle itself consists of two glass wires which are glued together at one side. This end is conical. Light will be submitted in the other end of one of the wires. The light will be reflected or emitted - depending on the phase (water respectively air) at the conical end. At the end of the other wire there is an detector which transforms the optical signal into an electrical one. Fig. 6 shows typical signals as they have been detected during a pre-test in which air has been pressed through a downwards facing horizontal plate. A level defines the period of time in which gas appears at the end of the probe t_g. By dividing this time period by the total observation time t one gets the time averaged local void fraction ε, which is plotted as a function of the height in Fig. 6 and is defined according Eq. (1):

$$\varepsilon = \frac{t_g}{t} \qquad (1)$$

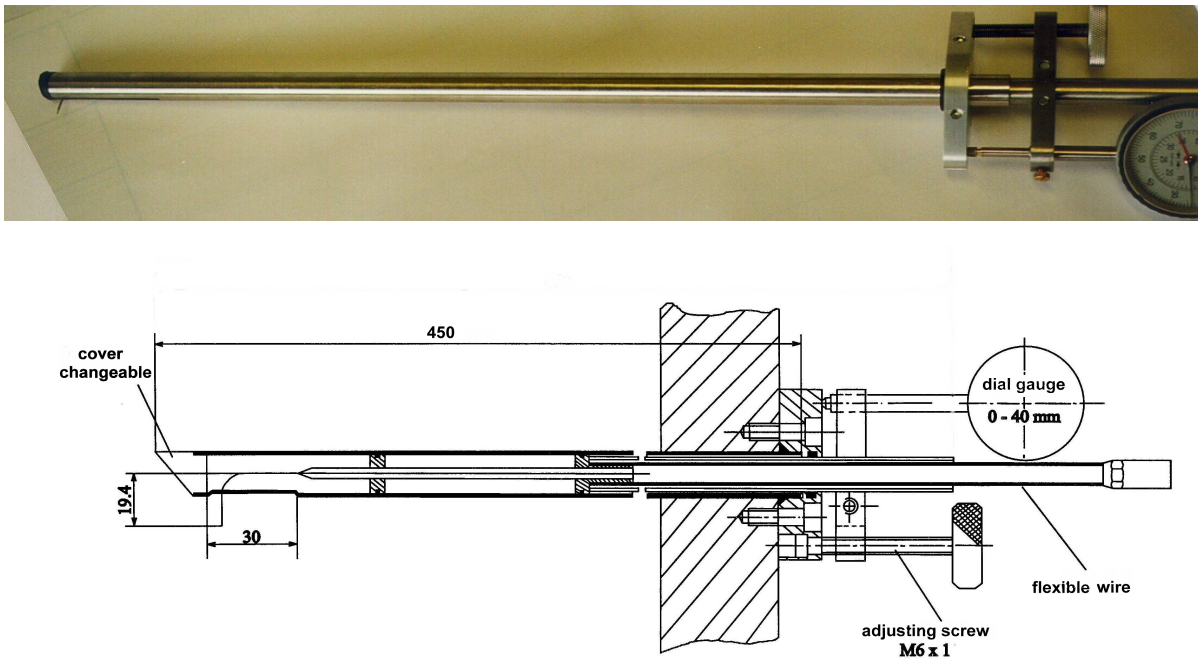

Fig. 5: Fiber optical needle probe

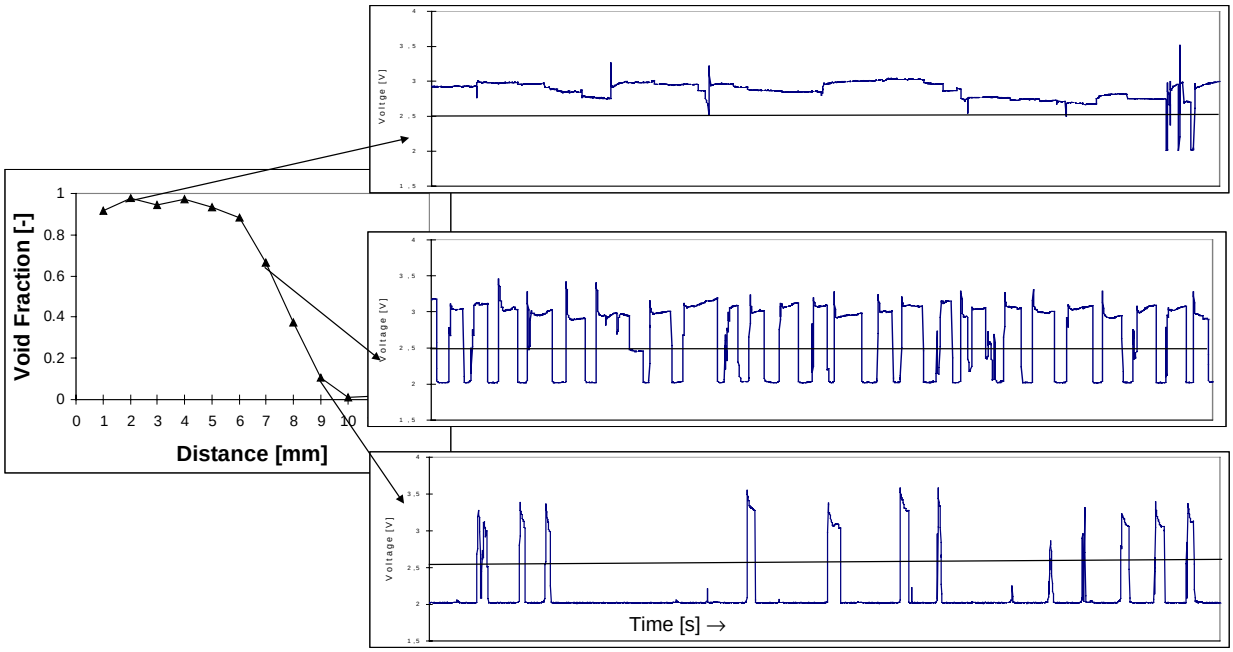

Fig. 6: Local void fraction determination

The fiber optical needle probe has been mounted at two different positions in the global model. The needle itself points into the main flow direction with the effect that the wires will have a minor influence on the measurement of the void fraction. In contrast to pre-tests with an inclination of 0° the void fraction distribution is flatter and almost linear as Fig. 7 shows.

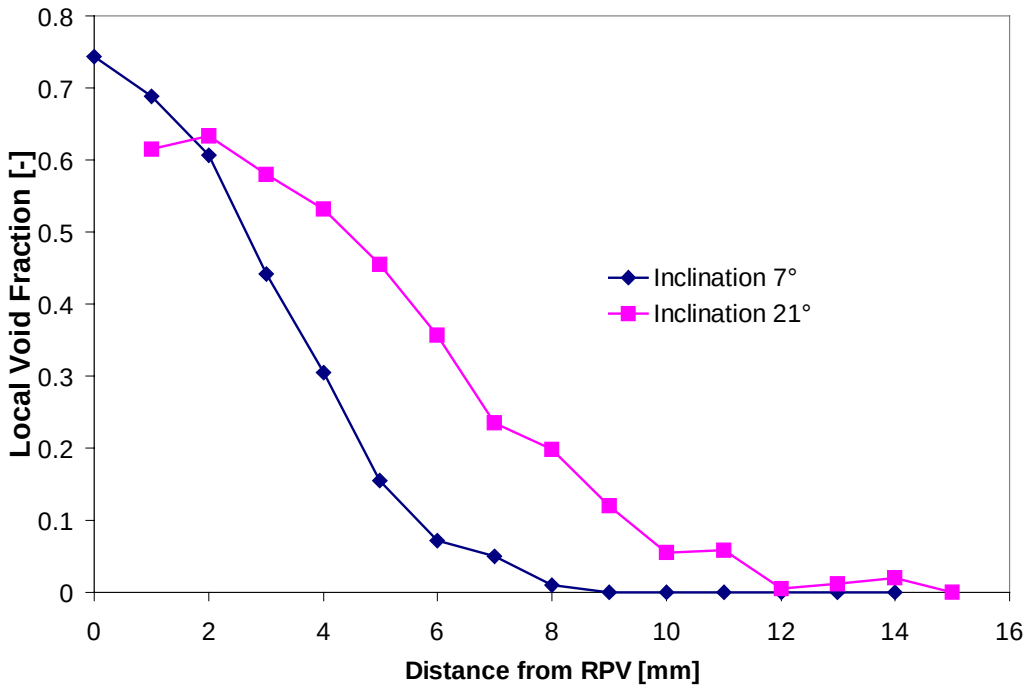

Fig. 7: Local void fractions at different inclinations

4.2 Impedance probes measurements

One quarter of the simulated CRD-drive houses has been replaced by electrodes of the same shape as the transparent bars. The electrical capacity has been measured for all pairs of neighboring electrodes - for single-phase water C_l, single-phase gas C_g and for the two-phase flow mixture C. The volume averaged void fraction $\bar{\varepsilon}$ is:

$$\bar{\varepsilon} = \frac{C - C_g}{C_l - C_g} \quad (2)$$

if one assumes that the void fraction distribution as a function of the height is equal in the whole area between the neighboring electrodes. The void fraction according Eq. (2) is an average over the whole gap between insulation and RPV. In this region a counter-current flow occurs with single-phase water flow along the insulation and two-phase flow along the RPV. To get an impressive description of the such a void fraction it is attractive to transform it into a geometrical value like the gas height h_g, which is described by the height of the whole gap h according Eq. (3):

$$h_g = \bar{\varepsilon}\, h \quad (3)$$

The gas height is supposed to be similar to the integration of the local void fraction over the height according to Eq. (4):

$$h_g = \int_0^h \varepsilon \, dh \quad (4)$$

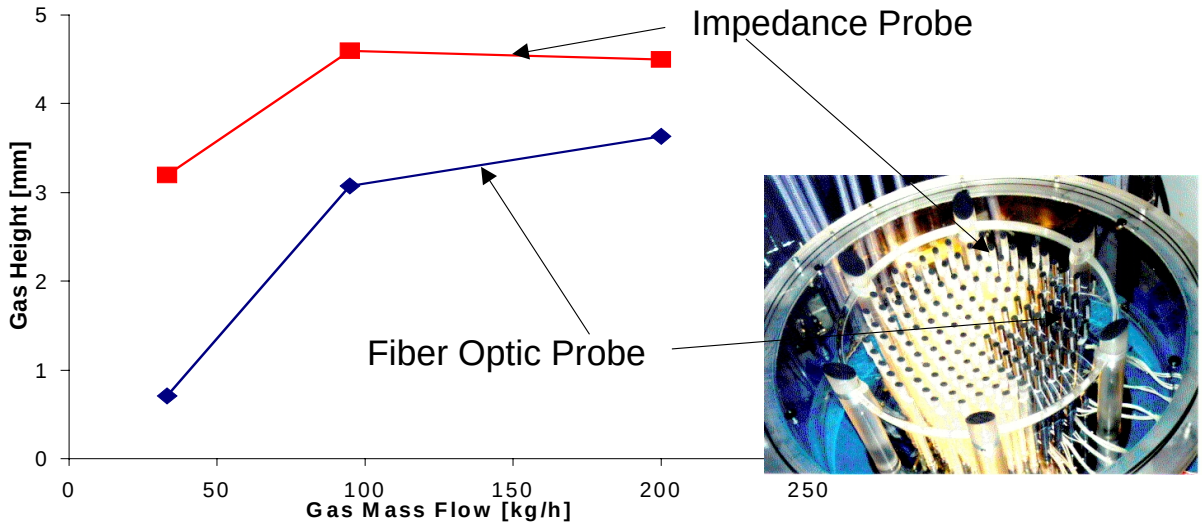

Fig. 8: Average gas height measured with fiber optical needle probe and impedance probes

Fig. 8 shows gas heights measured with impedance probes and the fiber optical needle probe as a function of different injected gas mass flows. The measurements

with the impedance probes deliver a little bit higher gas heights as the measurements with the fiber optical needle probe. This can be explained by the local flow conditions around the control rod drive housings. The needle probe has to be installed in the main flow direction, as explained in chapter 4.1. The pair of impedance probes, which delivers a gas height comparable to the needle probe, has to be in the line of the main flow direction. The visual observation proves, that the gas is pilled up in front of the control rod drive housings, whereas the gas level seems to be a little lower behind the control rod drive housings. These local flow conditions will have two effects. First, the gas height delivered by the impedance probes is a bit to high. Second, the gas height estimated by the fiber optical needle probe is a bit lower than the average gas height between the electrodes. This interpretation, together with the fact that the absolute differences between the gas height curves of Fig. 8 are small, prove the functioning of both void fraction measurement methods. In addition one can assume a higher accuracy for the gas height measurement with the impedance probes for pairs of electrodes which are orientated normal to the main flow direction.

All impedance probes together deliver a gas height distribution in a 90° sector of the model, as it is shown in Fig. 9. The colours of the squares in Fig. 9 represent the gas height between two neighboring control rod drive housings marked by circuits. The gas heights are almost rotational symmetrical distributed, which underlines the visual observation according chapter 2.1.

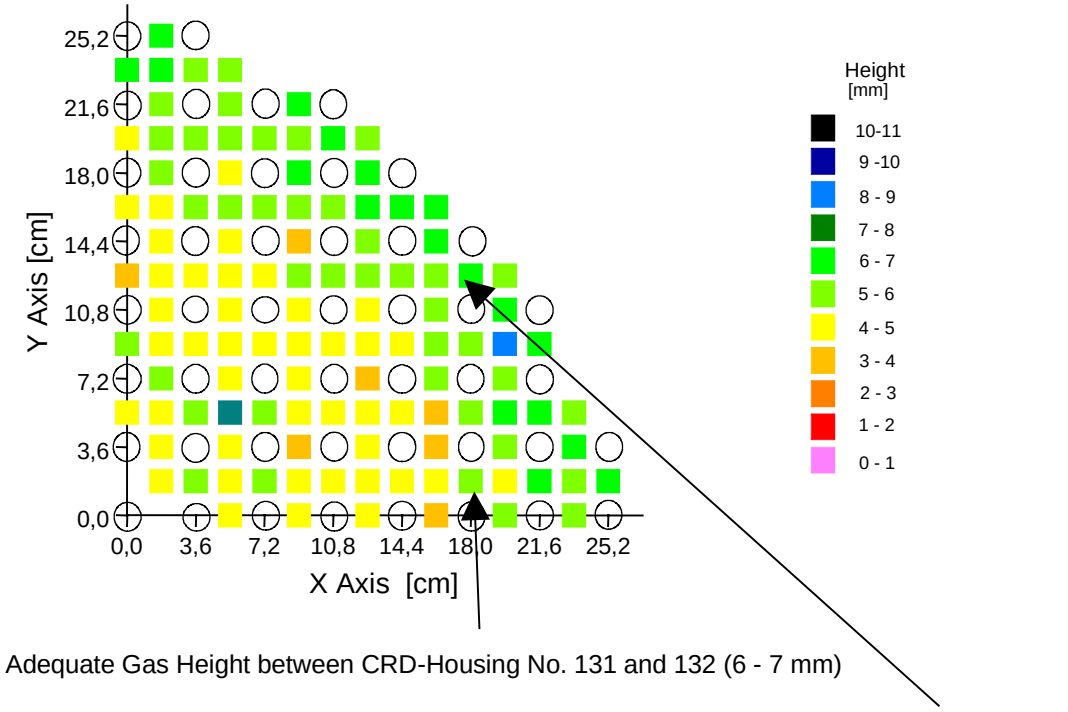

Fig. 9: Gas height distribution

4.3 Laser-Doppler Anemometer measurements

Nowadays Laser-Doppler Anemometers (LDA) are commercial available. Their main application is the measurement of single-phase flow velocities. The theoretical background of this technique is described in publications like /15/. The LDA, which has been used during the described tests, is a product of *Dantec Measurement Technology* (see background figures under www.dantecmt.com). In the following the way how a LDA works is described - so far it is necessary for the handling of the complete system and the interpretation of the results.

The functioning of a LDA is based on the Doppler principle - as the name indicates. Two laser beams (monochromatical and unipolar light) with a defined shift frequency will be focused via an optical system. The beams form an ellipsoidal volume when they are crossing each others. The reflection of a tracer particle crossing this volume will be detected by a photo multiplier. The frequency of the reflected light is proportional to the velocity of the tracer particle, which will be calculated by a computer.

The LDA-system delivers values for the velocity of tracer particles. The definition of the test procedure, the interpretation and the plausibility tests depend on each individual application. In the following part some of the activities are mentioned to get reliable values for the velocity around the RPV.

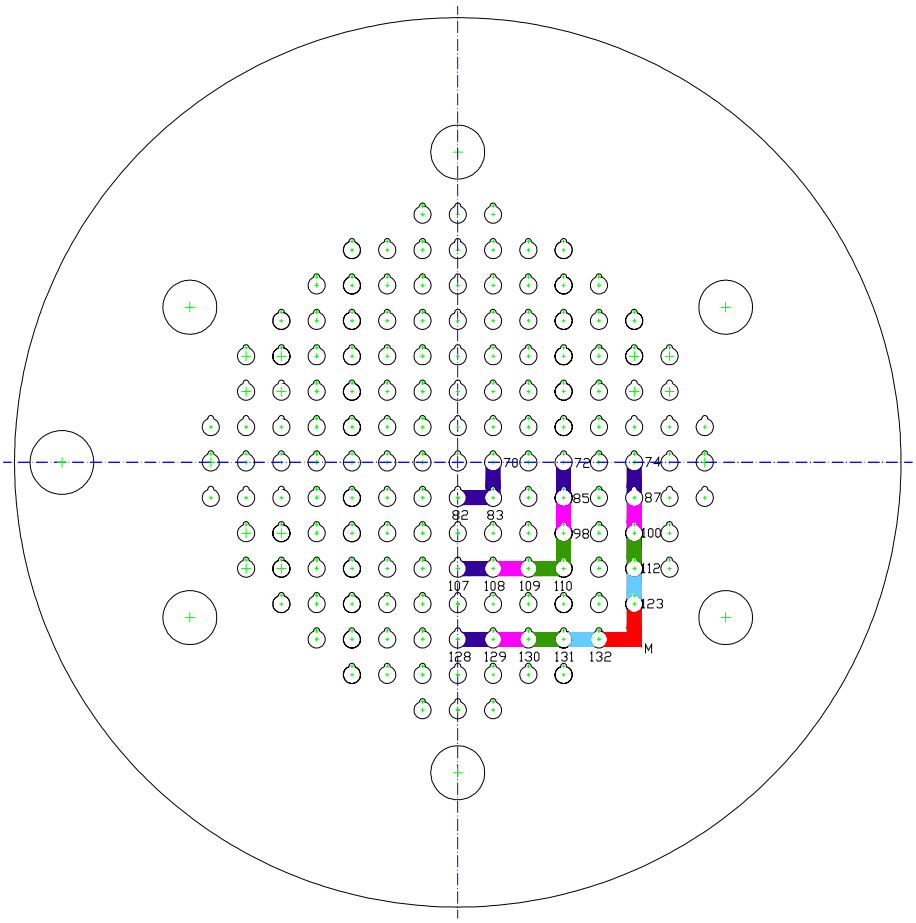

Fig. 10: Positions of the LDA measurements

4.3.1 Test procedure

The flow around the RPV is highly turbulent. For that reason it was necessary to measure some hundreds of velocities at one position to get the real average value. The optical system of the LDA has been moved from a position below the model in the upwards direction. Based on these measurements it was possible to get a velocity profile as a function of the height. The position of each measurement profile is shown in Fig. 10. It is always in the middle between two neighboring control rod drive housings. The measured velocities are normal to a line between the neighboring control rod drive housings and are almost similar to the average values on this line – this has been tested by measuring the velocities along this line at different heights.

The refraction of the laser beams influences not only the position of the measuring volume but also the length of this volume - increased by 50%. This has been taken into account when the optical system was positioned. The increased length of the volume must be considered during the interpretation of the measured velocities.

4.3.2 Interpretation of the velocities

Fig. 11 shows velocity profiles as a function of the height. Typical for these profiles are areas with negative velocities, which indicate a flow along the insulation to the vertex, and positive ones, which indicate a flow along the RPV out of the lower part of the gap between insulation and RPV. The absolute values of the average velocities in the negative area are lower than the ones in the positive area. This is plausible. The negative velocities occur in an area with only single-phase flow water, whereas a two-phase flow mixture occurs in the area with positive velocities. The air will accelerate the water and is herewith responsible for the higher velocities in the area with positive velocity. The measured velocities are water velocities, as plausibility tests proved (see chapter 4.3.3).

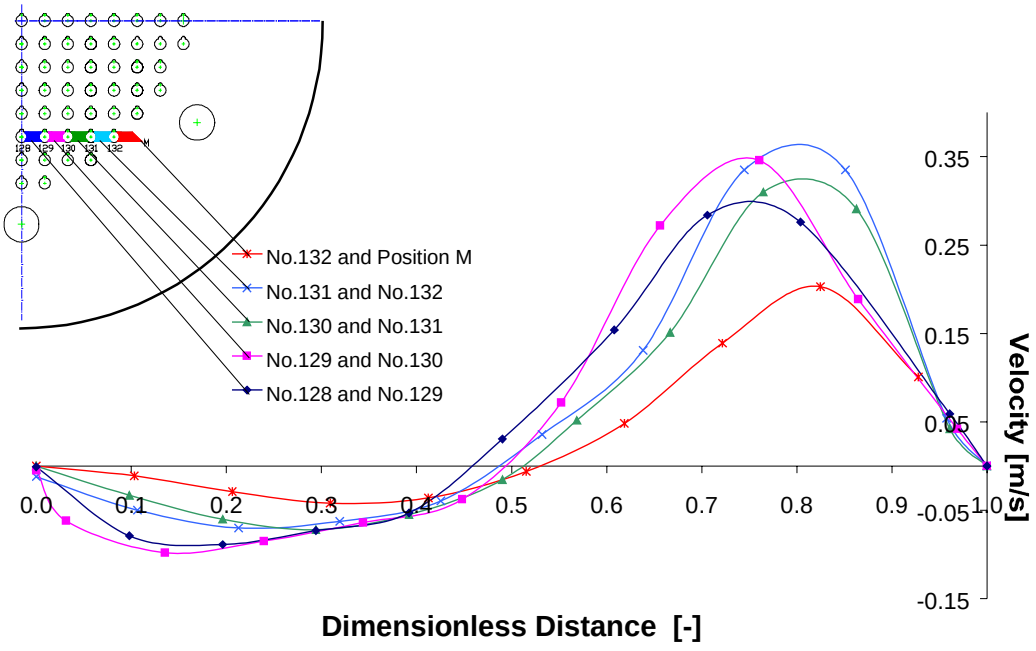

Fig. 11: Velocity distribution as the function of the height

The flatness of the profile is unusual, especially close to the boundaries. The relative long measuring volume is responsible for this effect. Each velocity delivered by the LDA-system is related to the center position of the measuring volume. In reality this value is the one of the average velocity within the length of the measuring volume. According /16/ the probability $p(x)$, that the reflection of the light at a particle occurs at the position *x* with a distance of $x - x_0$ from the center position of the measuring volume x_0, is proportional to the intensity of the laser $I(x)$ and the velocity $v(x)$:

$$p(x) \sim I(x) \cdot v(x) \tag{5}$$

The intensity of the light is according /16/ proportional to a Normal distribution, which is related to the length of the measuring volume Δx:

$$I(x) \sim \frac{1}{2 \cdot \Delta x \sqrt{\frac{\pi}{2}}} \exp\left(- \frac{2(x - x_0)^2}{(2 \cdot \Delta x)^2} \right) \tag{6}$$

From Eq. (5) and (6) follows Eq.(7) for the measuring volume averaged velocity delivered by the LDA-system:

$$\bar{v}(x_0) = \frac{\int_{x_0 - \Delta x}^{x_0 + \Delta x} p(x) \cdot v(x) \cdot dx}{\int_{x_0 - \Delta x}^{x_0 + \Delta x} p(x) \cdot dx} = \frac{\int_{x_0 - \Delta x}^{x_0 + \Delta x} I(x) \cdot v(x)^2 \cdot dx}{\int_{x_0 - \Delta x}^{x_0 + \Delta x} I(x) \cdot v(x) \cdot dx} \tag{7}$$

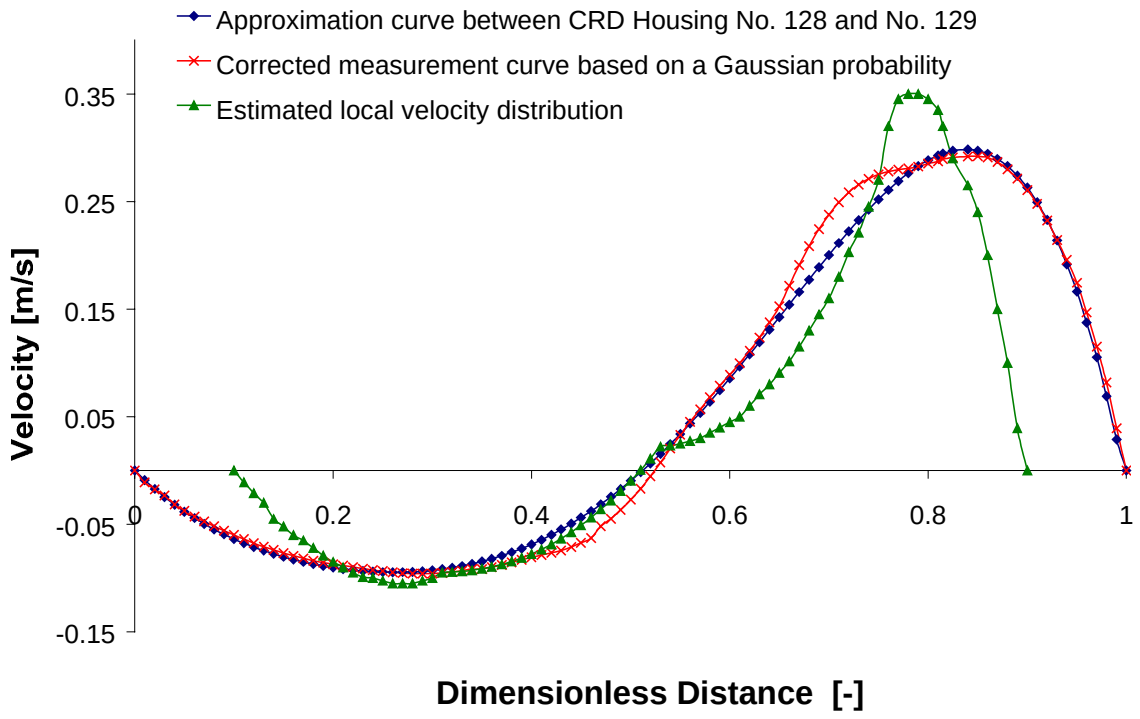

Fig. 12: Local velocities

Fig. 12 shows the local velocity and the averaged velocity profile as it is delivered by the LDA-System and which has been approximated by a polynominyl. One difference is the length of the profiles, which in the case of the local velocities is equivalent to distance between RPV and insulation and which in the case of the averaged velocities is longer. The difference in the length of the profiles is the length of the measuring volume. Another difference is the velocity gradient at the boundaries, which is higher in the case of the local velocities. This is plausible.

4.3.3 Plausibility check

Each of the measurement techniques itself is not new, but their combined application – especially the measurement of the water velocity in the two-phase flow area. For that reason it is essential to perform mass balances as a form of a plausibility check.

The visual observation, the gas height distributions and all velocity measurements together indicate that the flow is almost rotational symmetrical. For that reason it is possible to perform the mass balances based on the velocities between two control rod drive housings with the distance *b*. This means that the water mass balance across the area with negative velocities has to be the same as the water mass balance across the area with the positive values, according to Eq. (8) which represents a numerical integration:

$$\dot{M}_{W;in} = \left\{ \sum_{i=1}^{\substack{\text{Number of positions} \\ \text{in the area with} \\ \text{negative velocities}-1}} \left[\left(x_{i+1} - x_i\right) \left(v_i \left(\varepsilon_i - 1\right) + v_{i+1} \left(\varepsilon_{i+1} - 1\right)\right) \rho_L \frac{1}{2} \right] \right\} b \,(-1) \overset{!}{=}$$

$$\dot{M}_{W;out} = \left\{ \sum_{i=1}^{\substack{\text{Number of positions} \\ \text{in the area with} \\ \text{positive velocities}-1}} \left[\left(x_{i+1} - x_i\right) \left(v_i \cdot \left(\varepsilon_i - 1\right) + v_{i+1} \cdot \left(\varepsilon_{i+1} - 1\right)\right) \rho_L \frac{1}{2} \right] \right\} b \qquad (8)$$

The void fraction in the area with negative velocities is zero, whereas the distribution of the void fraction in the area with positive velocities is almost linear as a function of the height (Fig. 7 indicates the plausibility of the linear approach). The form of the linear profile can be described by the following two assumptions. First, the void fraction is zero at the defection point of the velocity profile. Second, the integration over the height according to Eq. (4) is the gas height measured with the impedance probes at this position. Based on these assumptions it is possible to check the water mass balance based on Eq. (8).

The gas mass balance has to be performed indirectly. This means, it can be checked whether the effect of the injected gas mass flow, which has been measured, is plausible. An approach is to assume that the area between two control rod drive housings might be described as two channels – one for the area with positive and one for the area with negative velocities. The void fraction in the upper channel is the ratio of the gas height to the velocity deflection point h_2 :

$$\varepsilon = \frac{h_G}{h_2} \qquad (9)$$

It is possible to predict the void fraction in such inclined channels according the Chexal-Lellouche /17/ correlation. This correlation requires as a kind of input values the properties, the inclination, the hydraulic diameter (which is in this case $d_h = 2\,b\,h_2\,/(b+h_2)$) and the superficial velocities of gas and liquid. Fig. 13 shows the void fractions calculated with the Chexal-Lellouche correlation. The superficial velocity of the water is the ratio of the inlet water mass flow of Eq. (8) and the cross section. The gas superficial velocity has been varied. The gas mass flow in Fig. 13 is the superficial velocity multiplied by the cross section of the balance area. The red lines in Fig. 13 indicate the values of gas mass flows affecting void fractions which are equivalent to the measured (defined according Eq. (9)).

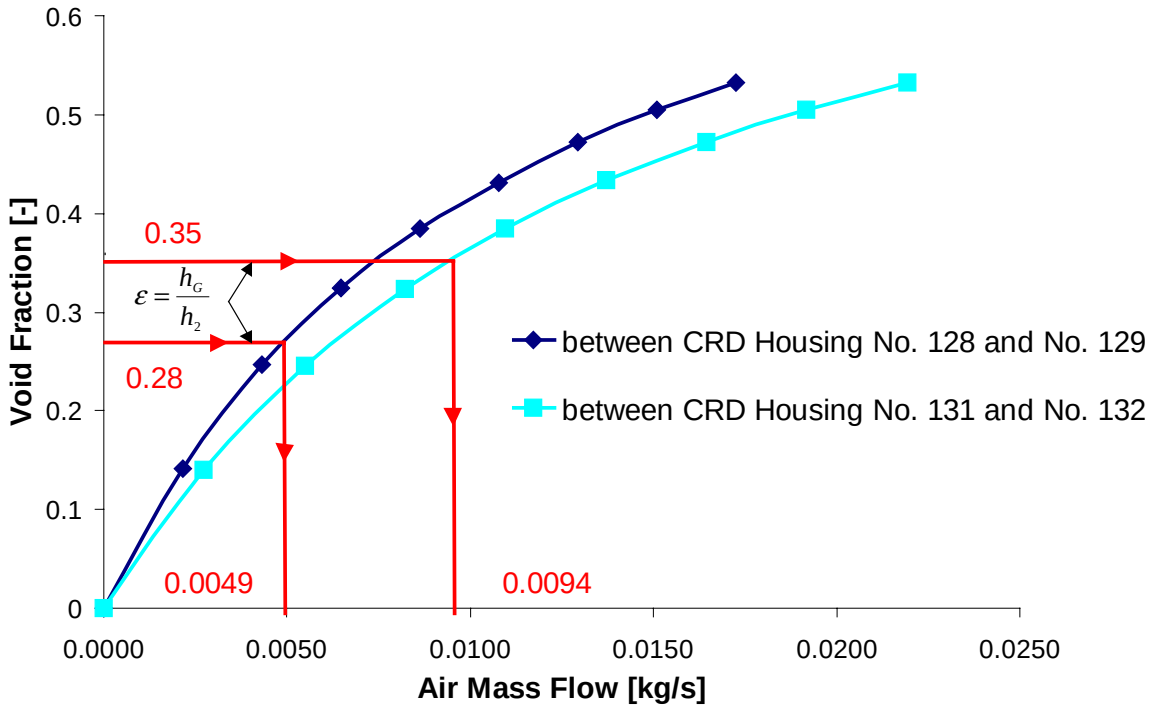

Fig. 13: Gas mass flow balance

Fig. 14 contains the results of mass balances performed at two positions. The accuracy is in the range of 20%, which is a good agreement for two-phase flow conditions. The main conclusion is, that the interpretation of the measurements is plausible.

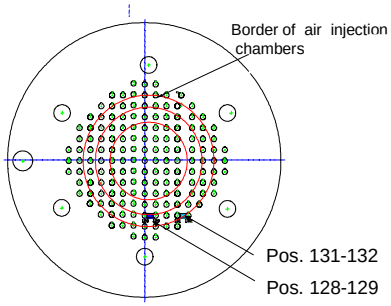

	Position 128-129	Position 131-132
Water Mass Flow, Inlet [kg/s]	1,19	1,36
Water Mass Flow, Outlet [kg/s]	1,40	1,59
Ratio Water Mass Flow Out/In	1,18	1,17
Air Mass Flow, Injected [kg/s]	0,0043	0,0085
Air Mass Flow, Acc. Fig. 13 [kg/s]	0,0049	0,0094
Ratio Out/In	1,14	1,11

Fig. 14: Results of the mass balances

4 Conclusions and outlook

It is the aim of the tests to investigate the flow conditions around the RPV for the case of a hypothetical accident with core melting. Three different measurement techniques have been used for this purpose. The test in the global model have been compared with measurements in section models and the similarity of the flow conditions could be demonstrated. Based on this comparison it was possible to find the size of a section with almost similar flow conditions as they occur in the case of the flow around the whole RPV.

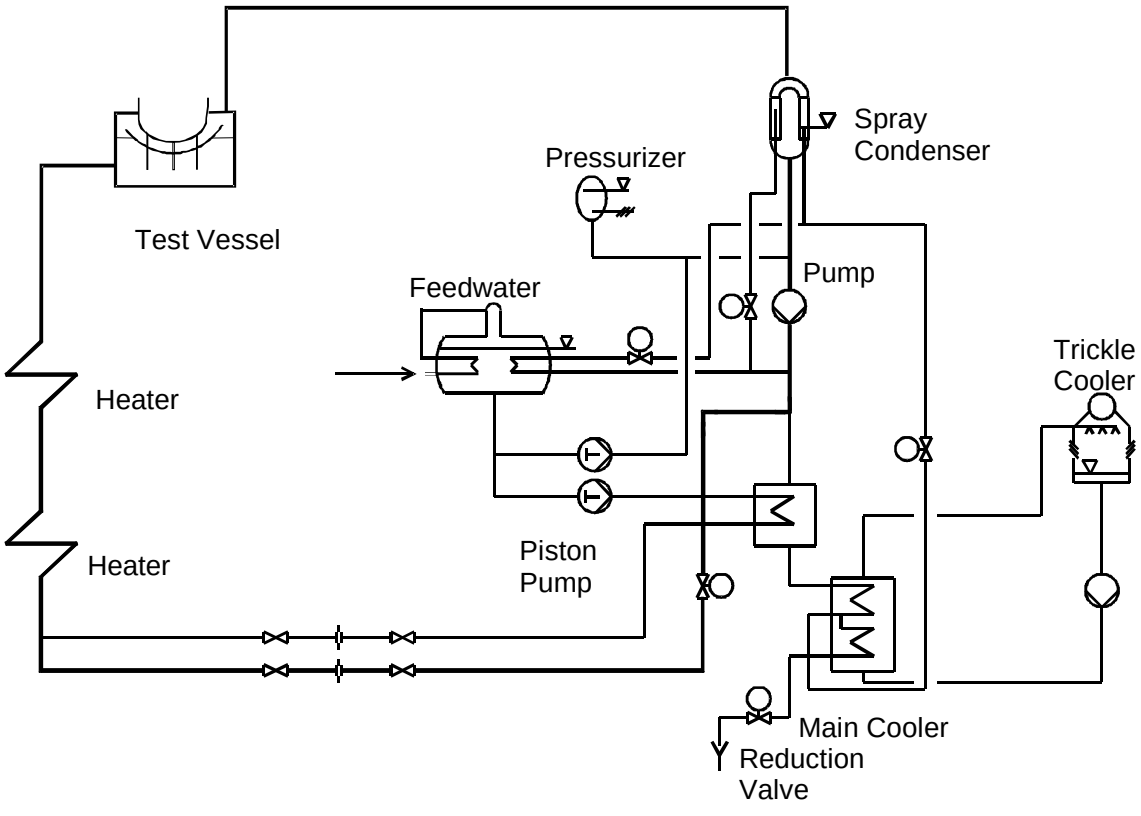

Fig. 15: Measurement of safety margins with the BENSON test rig

In addition, the measurements are the data base to adjust computer codes. VTT will use these codes to confirm the selected size of the heatable section. Such a section (1:1 scale) will be integrated into the BENSON test rig (see Fig. 15) which is a flexible separate effect test facility and which can be operated in the range of pressures from 1 to 330 bar, of fluid temperatures from 20 to 600°C, of mass flows up to 28 kg/s and of electrical heat capacities up to 2 MW. The heat flux will be increased until a boiling crisis occurs or a safety margin of 3 is reached.

To use a LDA to measure the velocity of the liquid phase in a water/air mixture is a new application for this technique. Therefore it was essential to prove the plausibility of these measurements. Water and air mass flow balances prove that the measurements are reliable.

Literature

/1/ Cheung F.B., Haddad K.H., Liu Y.C, Shia S.W., High Heat Flux Nucleate Boiling on the Outer Surface of a Heated Hemispherical Vessel, AICHe Symp. Ser. Vol. 93, No. 314, pp.95-101, 1997

/2/ Theofanous T.G., Liu C., Additon S., Angelini S. Kymäläinen O., Salmassi T., Invessel Coolability and Retention of a Core Melt, DOE/ID-10460 Vol. 1 and 2, October 1996

/3/ Henry R.E. and Fauske H.K., External Cooling of a Reactor Vessel under Severe Accident Conditions, Nuclear Engineering and Design, 139 (1993), pp. 31-43

/4/ Henry R.E. et al., Experiments on the Lower Plenum Response During a Severe Accident, Proc. 4th Int. Topical Meet. on Nuclear Thermal Hydraulics, Operations and Safety, Vol. 1, April 1994, pp. 27-C1-6

/5/ Theofanous T.G., Liu C., Additon S., Angelini S. Kymäläinen O., Salmassi T., Invessel Coolability and Retention of a Core Melt, Nuclear Engineering and Design, 169 (1997), pp. 49-57

/6/ Rouge S., SULTAN Test Facility, Large Scale Vessel Coolability in Natural Convection at Low Pressure, NURETH-7 Conf., Saratoga Springs, NY, USA, Sept. 10-15, 1995

/7/ Rouge S., Dor I. Geffraye G. Reactor Vessel External Cooling for Corium Retention, SULTAN Experimental Program and Modeling with CATHARE Code, OECD Workshop on IN-Vessel Debris Retention and Coolability, Garching, Germany, March 3-6, 1998

/8/ Theofanous T.G., Syri S., Salmassi T., Kymäläinen O., Tuomisto H., Critical Heat Flux through Curved, Downward Facing, Thick Walls, Int. Conf. on New Trends in Nuclear System Thermohydraulics, May 30th –June 2nd, 1994, Pisa, Proc. Vol. 2, pp. 585-597

/9/ Theofanous T.G. and Syri S., The Coolability Limits of a Reactor Pressure Vessel Lower Head, NURETH-7 Conf., Saratoga Springs, NY, USA, Sept. 10-15, 1995

/10/ Seiler J.M., Dossier de'analyse GAREC, Retention du corium en curve. Synthese, CEA STR/LTEM/96-42, pp. 140-174

/11/ Cheung F.B., Haddad K.H., A Hydrodynamic Critical Heat Flux Model for Saturated Pool Boiling on a Downward Facing Curved Heating Surface, Int. J. Heat Transfer, 40 (1997), pp. 1291-1302

/12/ Cheung F.B., Liu Y.C., Natural Convection Boiling on the Outer Surface of a Hemispherical Vessel Surrounded by a Thermal Insulation Structure, OECD Workshop on In-Vessel Debris Retention and Coolability, Garching, May 3-6,1998

/13/ Theofanous T.G., Yuen W.W., Fundamentals of Boiling and Multiphase Flow under Extreme Conditions, Heat Transfer 1998, Proceedings of the11th IHTC, Vol. 1, pp. 131-147, Kyongju, 1998

/14/ Benk H., Information zur Verwendung der faseroptischen Meßtechnik für Strömungsuntersuchungen im RDB-Modell zum SWR 1000, TU-Darmstadt, 1999

/15/ Durst F., Melling A., Whitelaw J.H., Theorie und Praxis der Laser-Doppler-Anemometrie, G.Bauer Verlag, Karlsruhe, 1987

/16/ Waßner E., Strömungsuntersuchungen mit der Laser-Doppler-Anemometrie bei der Extrusion von Polyethylenschmelzen, Shaker Verlag, Aachen, 1998

/17/ Chexal et. al., Void Fraction Technology for Design and Analysis, EPRI-Report TR-106326, March 1997